Environmental Pollution 290 (2021) 118051

Contents lists available at ScienceDirect

Environmental Pollution

journal homepage: www.elsevier.com/locate/envpol

Impact of North Atlantic-East Asian teleconnections on extremely high January PM_{10} cases in Korea☆

Jeong-Hun Kim [a,b], Seong-Joong Kim [b], Daeok Youn [c], Maeng-Ki Kim [a,*], Joo-Hong Kim [b], Joowan Kim [a], El Noh [a]

[a] Department of Atmospheric Science, Kongju National University, Gongju, 32588, Republic of Korea
[b] Division of Atmospheric Sciences, Korea Polar Research Institute, Incheon, 21990, Republic of Korea
[c] Department of Earth Science Education, Chungbuk National University, Cheongju, 28633, Republic of Korea

ARTICLE INFO

Keywords:
PM_{10} concentration
East asia winter monsoon
Wave propagation
Atmospheric teleconnection

ABSTRACT

In this study, we investigated the daily variability of PM_{10} concentrations in January in Korea during the past 19 years (2001–2019), as well as the associated atmospheric circulation patterns. The daily PM_{10} concentrations were classified into three cases: low (L; < 50 μg/m^3), high (H; 50–100 μg/m^3), and extremely high (EH; ≥ 100 μg/m^3). We found that the strength of the East Asian winter monsoon influenced the PM_{10} variability in the L and H cases. However, the EH cases were strongly influenced by the rapid growth of barotropic warming (anticyclonic anomaly) over the eastern North Atlantic and Northern Europe (ENE), and the stationary Rossby waves grew rapidly over Eurasia within only four days. Analysis of the quasi-geostrophic geopotential tendency budget revealed that the anticyclonic anomaly over the ENE was enhanced by vorticity advection. Linear baroclinic model experiments confirmed that vorticity forcing over the ENE induces favorable atmospheric conditions for the occurrence of EH PM_{10} events in East Asia. As a result, the PM_{10} concentration sharply increased sharply by approximately three times over four days. This study suggests that understanding atmospheric teleconnections between the ENE and East Asia can effectively predict the occurrence of EH PM_{10} events in Korea, helping to reduce the human health risks from atmospheric pollution.

1. Introduction

Over the last decade, high particulate matter (PM) concentration events in the winter season have occurred most frequently in East Asia (Wang et al., 2015; Wang and Chen, 2016; Cai et al., 2017; Kim et al., 2019). These events have increased the risk of cardiovascular and respiratory diseases (Brunekreef and Holgate, 2002; Nel, 2005) in China and Korea. A prime example was the high PM concentration event in January 2013 in China and Korea, referred to as *airpocalypse*, which caused significant damage (Park et al., 2013; Wang et al., 2014; Zou et al., 2017; Koo et al., 2018). In Beijing, this high PM episode in 2013 caused 476 acute deaths, equivalent to ~180 million dollars in damage or ~0.76% of the GDP (Du and Li, 2016). Since the early 2000s, the Korean government has continually reduced emissions from factories and various transportation types through the "National Environmental Comprehensive Plan" (Korea Ministry of Environment, 2015; Kim et al., 2016; Lee et al., 2020b; Bae et al., 2021), helping to decrease the national atmospheric PM concentration (Lee et al., 2020b; Oh et al., 2015). Nevertheless, high PM concentration events are stronger and more frequent in January (Jung et al., 2019; Kwon et al., 2020).

PM in which 50% of particles have an aerodynamic diameter less than 10 μm (PM_{10}) is mainly emitted by factories, cars, and power plants (Chen et al., 2013; Kim et al., 2016; Ryou et al., 2018; Rai et al., 2021). In particular, high PM_{10} pollution in Korea and China is affected by combined factors such as emission sources (Kim et al., 2016; Kim et al., 2017a, b), inflow from neighboring countries (Seo et al., 2018; Hur et al., 2021), and meteorological conditions (Dotse et al., 2016; Guan et al., 2017). PM_{10} emission sources can be classified into natural and anthropogenic (Kim et al., 2016; Seo et al., 2017), which are both affected by distinct sources and atmospheric circulation patterns (Lee et al., 2018; Jung et al., 2019). Yellow dust, a natural pollutant, is mainly transported by winds from the desert regions of northern China and Mongolia (Lee and Kim, 2018). However, PM_{10} is primarily caused by local emissions in South Korea, transport from China and North Korea

☆ This paper has been recommended for acceptance by Admir C. Targino.

* Corresponding author.
E-mail address: mkkim@kongju.ac.kr (M.-K. Kim).

https://doi.org/10.1016/j.envpol.2021.118051
Received 22 April 2021; Received in revised form 18 August 2021; Accepted 23 August 2021
Available online 25 August 2021

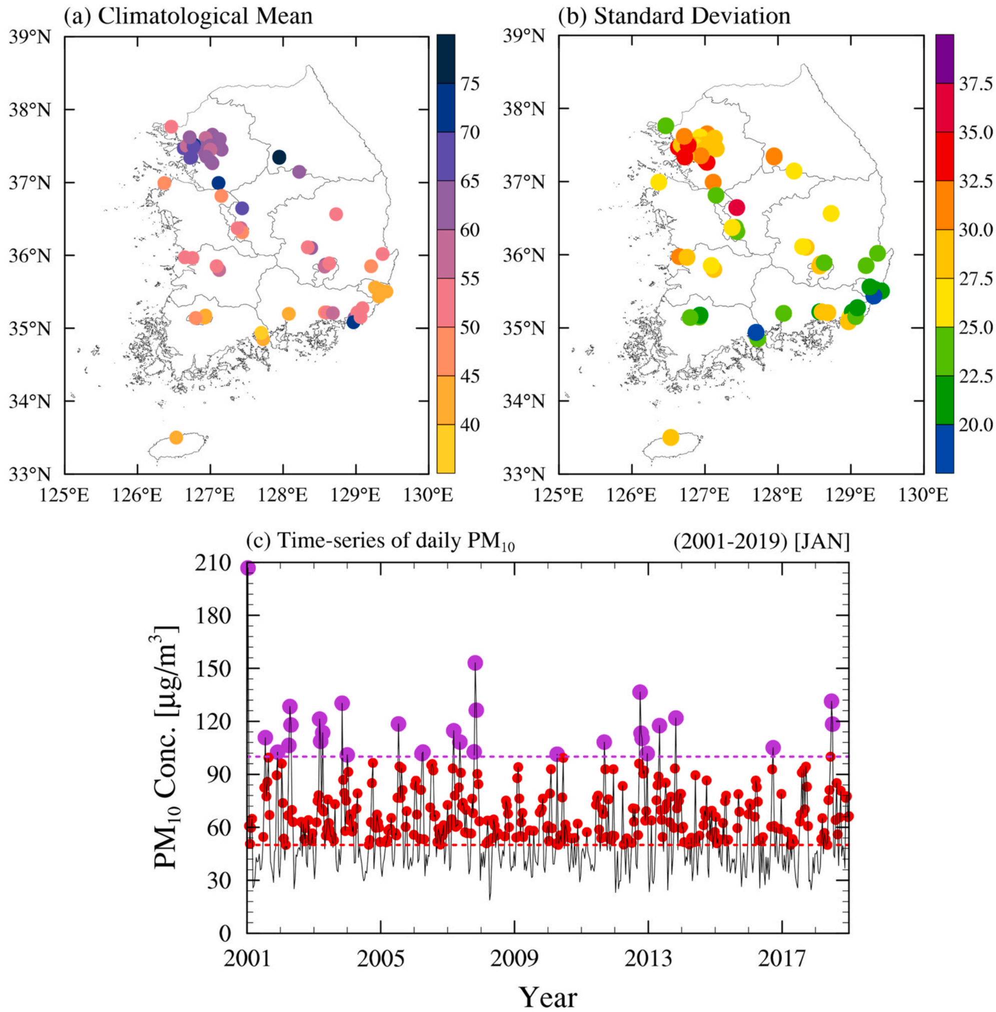

Fig. 1. The spatial distribution of (a) climatological mean, (b) standard deviation, and (c) the time-series of January PM_{10} concentrations over 19 years (2001–2019). The red and purple circles in (c) indicate H cases (50–100 μg/m^3) and EH cases (≥100 μg/m^3), respectively. The red and purple dashed lines indicate 50 and 100 μg/m^3, respectively. (For interpretation of the references to colour in this figure legend, the reader is referred to the Web version of this article.)

(Lee et al., 2013; Kim et al., 2016), and weakening dispersion by stagnant atmospheric circulation patterns (Seo et al., 2018; Shi et al., 2019; Oh et al., 2020). The stagnant atmospheric circulation pattern that influences the high PM_{10} concentration events in East Asia reduces the dispersion of PM_{10} pollutants by strengthening the horizontal and vertical atmospheric stability (Lee et al., 2011; Zou et al., 2017; Kim et al., 2019; Kwon et al., 2020).

Stagnant atmospheric circulation patterns are affected by various teleconnections. Previous studies have suggested that a weakening of the East Asian winter monsoon (EAWM) induces stagnant atmospheric circulation, a much shallower boundary layer height, and stable atmospheric stratification, resulting in increased aerosols and PM_{10} concentrations in China and Korea (Niu et al., 2010; Kim et al., 2016; Jeong and Park, 2017). In addition, the Siberian high pressure and Aleutian low pressure are the dominant surface pressure systems in East Asia that determine the wind direction and wind speed during the winter season associated with the EAWM; the variability in these systems can therefore lead to high PM_{10} pollution in East Asia (Oh et al., 2018; Kim et al., 2019). A decrease in Arctic sea ice concentration and Eurasian snow cover has been suggested to weaken the Siberian high pressure, which suppresses the northerly winds and induces a stagnant atmospheric circulation pattern in China and the Korean Peninsula, causing high PM_{10} concentration events during the winter season (Wang et al., 2015; Zou et al., 2017; Kim et al., 2019). Lee et al. (2020b) found that the weakening of the Ural blocking since 2014 suppressed cold air flows from the north, causing favorable atmospheric conditions for poor air quality in East Asia. In addition, it was reported that the El Niño–Southern Oscillation (ENSO) alters the haze days by modulating winter precipitation in northern China (He et al., 2019). The El Niño event reduces wet deposition and induces haze events. The PM_{10} concentration on the Korean Peninsula is also closely related to the precipitation change caused by ENSO (Wie and Moon, 2017). However, the relationship between North Atlantic forcing and the high PM_{10} pollution in East Asia is relatively unknown.

We hypothesize that remote forcing over the North Atlantic may play an important role in triggering extremely high PM_{10} events in East Asia. Knowing this information in advance can minimize the health impacts caused by extremely high PM_{10} episodes. Therefore, this study examined the teleconnection between North Atlantic forcing and stagnant atmospheric patterns associated with the occurrence of high PM_{10} events during January 2001–2019 in Korea. Atmospheric variability is typically higher in January, mainly due to the influence of a strong or weak EAWM (Zhao et al., 2018). However, as the impact of yellow dust on PM_{10} concentrations is relatively small and high PM_{10} events are most frequent (Jung et al., 2019; Kwon et al., 2020; Ku et al., 2021), January is considered an ideal month for studying the impact of atmospheric

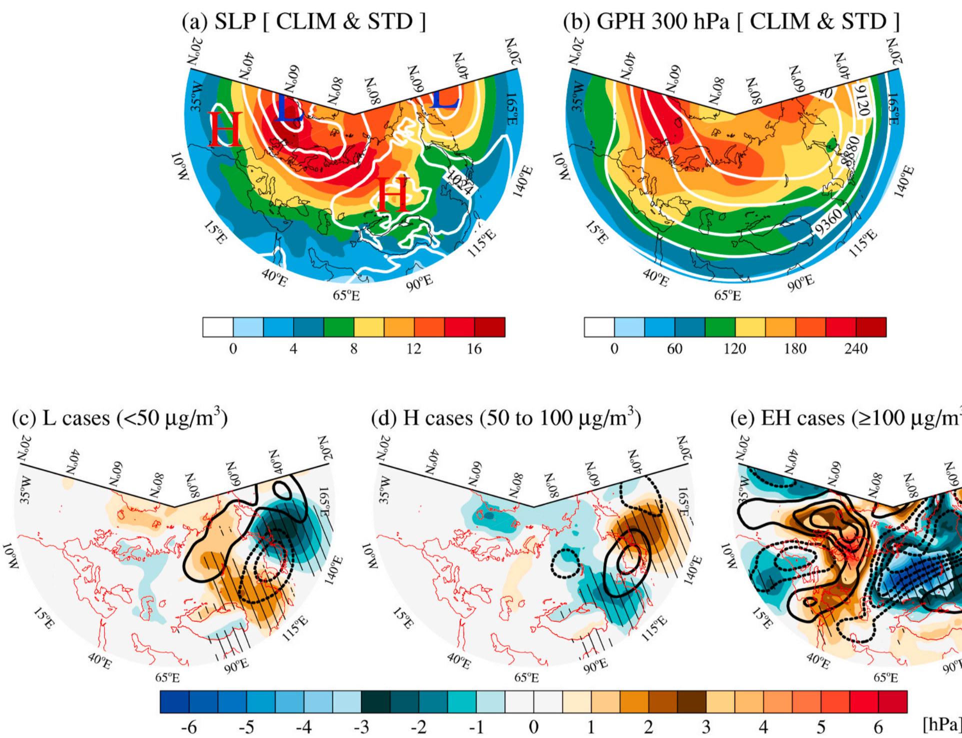

Fig. 2. (a–b) Climatological mean (white contour) and standard deviation (shading) of (a) sea level pressure (SLP; contour interval of 4 hPa) and (b) upper-level (300 hPa) geopotential height (GPH; contour interval of 240 m). (c–e) Composite anomalies of the January SLP (shading) and GPH at 300 hPa (contour interval of 20 m; dashed contours are negative) for L (<50 μg/m^3), H (50–100 μg/m^3), and EH (≥100 μg/m^3) cases, respectively. The hatched areas indicate a 10% significance level for SLP.

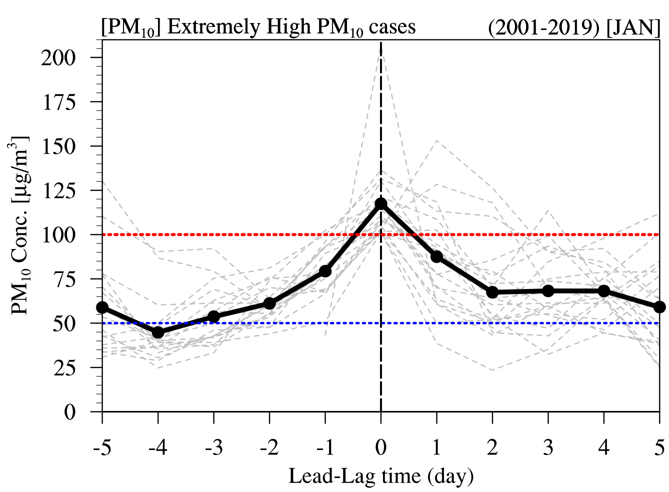

Fig. 3. Lead-lag time series of PM_{10} concentrations from five days before to five days after the occurrence of EH cases. The black solid line indicates the mean PM_{10} concentration, and the gray dashed lines indicate the PM_{10} concentration of each EH case. The red and blue dashed lines indicate PM_{10} concentrations of 50 μg/m^3 and 100 μg/m^3, respectively. (For interpretation of the references to colour in this figure legend, the reader is referred to the Web version of this article.)

circulation on PM_{10} variability. We employed statistical methods to define extremely high PM_{10} cases and identify atmospheric circulation patterns associated with extreme cases. In addition, we applied a dynamical method and modeling to understand the teleconnection mechanisms between the anticyclonic anomaly over the North Atlantic and the stagnant atmospheric conditions in Korea associated with extremely high PM_{10} episodes.

2. Methods

2.1. Observation and reanalysis data

In this study, we used daily PM_{10} data collected over 19 years (2001–2019) from 68 observational stations provided by the National Institute of Environmental Research (NIER), Korea (https://www.airkorea.or.kr) (Fig. 1a). To ensure the statistical reliability of the data, 68 stations, which possess more than 70% of the January data during the analysis period, were used in this study. According to Yellow dust day information provided by Korean Meteorological Administration (KMA), we excluded Yellow dust days from the analysis. Thus, PM10 data do not represent Yellow dust. Daily data were obtained by averaging the hourly PM_{10} concentration data.

ERA-interim reanalysis data provided by the European Centre for Medium-Range Weather Forecasts (ECMWF) were used to investigate atmospheric circulation patterns associated with high PM_{10} concentrations in Korea. The horizontal resolution of the data was 1.5° × 1.5° with 37 pressure levels. Our analysis of atmospheric circulations focused on the lower- (1000 and 850 hPa) and upper-level (300 hPa) geopotential height (GPH). The main variables used in the analysis were surface air temperature (SAT), sea level pressure (SLP), surface pressure (SP), GPH, air temperature (TMP), relative humidity (RH), specific humidity (SH), relative vorticity (RV), planetary boundary layer height (PBLH), horizontal wind (U- and V-wind), surface horizontal wind (Vsfc), and vertical velocity (W-wind).

2.2. Classification and composite analysis

In this study, we used the median and the 95th percentile values to classify the January PM_{10} concentrations in Korea during the past 19 years. The daily PM_{10} concentration were divided into three classes. In addition, we applied a composite analysis to determine the temporal evolution of daily weather patterns associated with high PM_{10} pollution

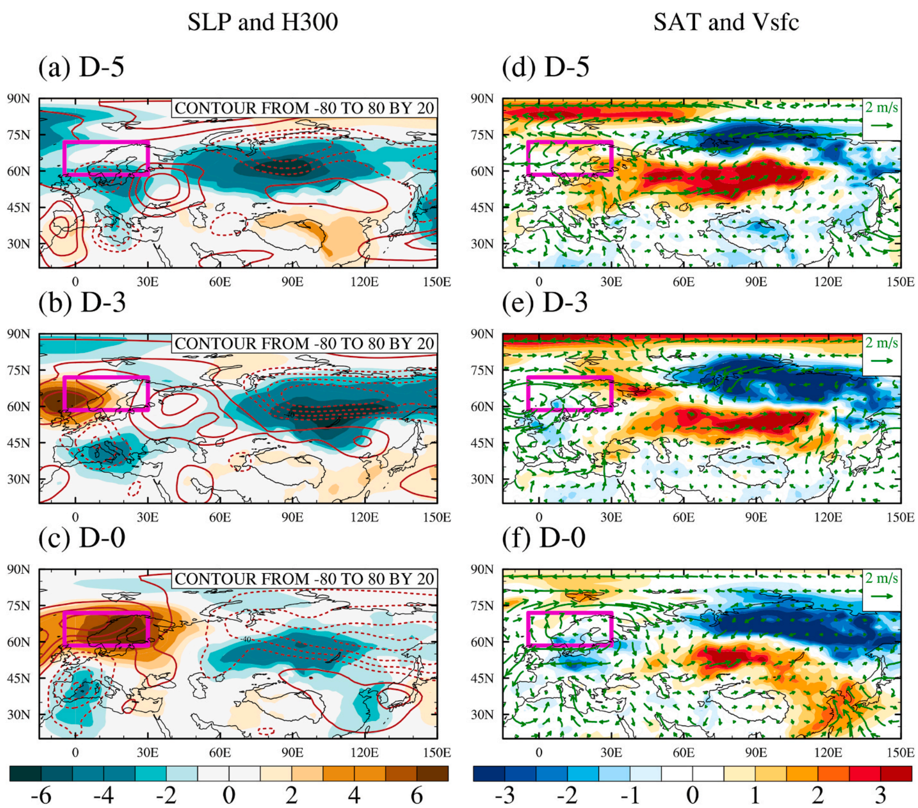

Fig. 4. Composite anomalies of January (a–c) sea level pressure (SLP; units: hPa; shading) and upper-level (300 hPa) geopotential height (GPH; units: m; contour interval of 20 m, dashed lines are negative), and (d–f) surface air temperature (SAT; units: K; shading) and surface winds (Vsfc; vectors) before and during the occurrence of EH cases. The pink boxes indicate the eastern North Atlantic and Northern Europe (ENE; 58.5 °N to 72 °N, 4.5 °W to 30 °E). (For interpretation of the references to colour in this figure legend, the reader is referred to the Web version of this article.)

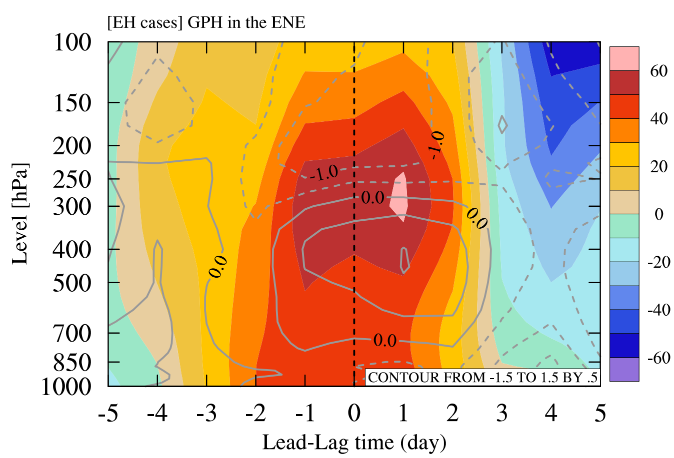

Fig. 5. Vertical distribution of the composite anomaly of geopotential height (GPH; shading; units: m) and temperature (TMP; contour interval of 0.5 K; units: K; dashed contours are negative) in the eastern North Atlantic and Northern Europe (ENE; 58.5 °N to 72 °N, 4.5 °W to 30 °E) before and after the occurrence of EH cases. The black dashed line indicates the start day of EH cases.

in Korea.

2.3. *Wave activity flux analysis*

The three-dimensional wave activity flux (WAF) was calculated according to the formula of Takaya and Nakamura (2001). The WAF is useful diagnostics for Rossby wave's energy propagation and related teleconnection. Rossby waves in the upper troposphere are associated with large-scale meanders of the jet stream, that are important in modulating atmospheric circulation patterns in the troposphere, including the planetary boundary layer. Therefore, we analyzed the WAF to confirm the stationary Rossby waves from the North Atlantic forcing, which is related to the high PM_{10} cases in Korea, as described in section 3.2.

2.4. *Quasi-geostrophic geopotential tendency budget*

The quasi-geostrophic geopotential tendency (QG tendency) equation was calculated following the method by Holton (2004). The QG tendency budget analysis is a helpful tool for quantitatively evaluating the contribution of dynamical processes (three forcing terms) to the temporal evolution of stationary high pressure (Hwang et al., 2020). The three forcing terms of the QG tendency equation are vorticity advection (F_{vort}), temperature advection (F_{heat}), and diabatic heating (F_{diab}). The total forcing (F_{ALL}) is defined as the sum of F_{vort}, F_{heat}, and F_{diab}. In this study, the cause of the rapidly developed anticyclonic anomaly in the North Atlantic that affects the high PM_{10} pollution in Korea (as described later) was analyzed through each forcing of the QG tendency.

2.5. *Linear baroclinic model description*

A linear baroclinic model (LBM) developed by Watanabe and Kimoto (2000) was used to confirm the effect of forcing on the change in GPH and to examine the steady atmospheric response to forcing (e.g., vorticity and heating) over targeted regions. The LBM used in this study had a dry dynamical core and is based on primitive equations linearized about a basic state on a sphere. The LBM consisted of a horizontal resolution of the T42 Gaussian grid and 20 vertical levels of sigma coordinates. The T42 is a 128 × 64 regular longitude/latitude global horizontal grid (approximately 2.8° resolution). The primary forces in the LBM are diabatic heating, vorticity, and divergence. In this study, we used the diagnosed forcing fields derived from reanalysis data. Further details of the model equations can be found in Watanabe and Kimoto (2000). The model experiment was integrated for 50 days, and the results are presented as the average of 10 days after reaching a steady

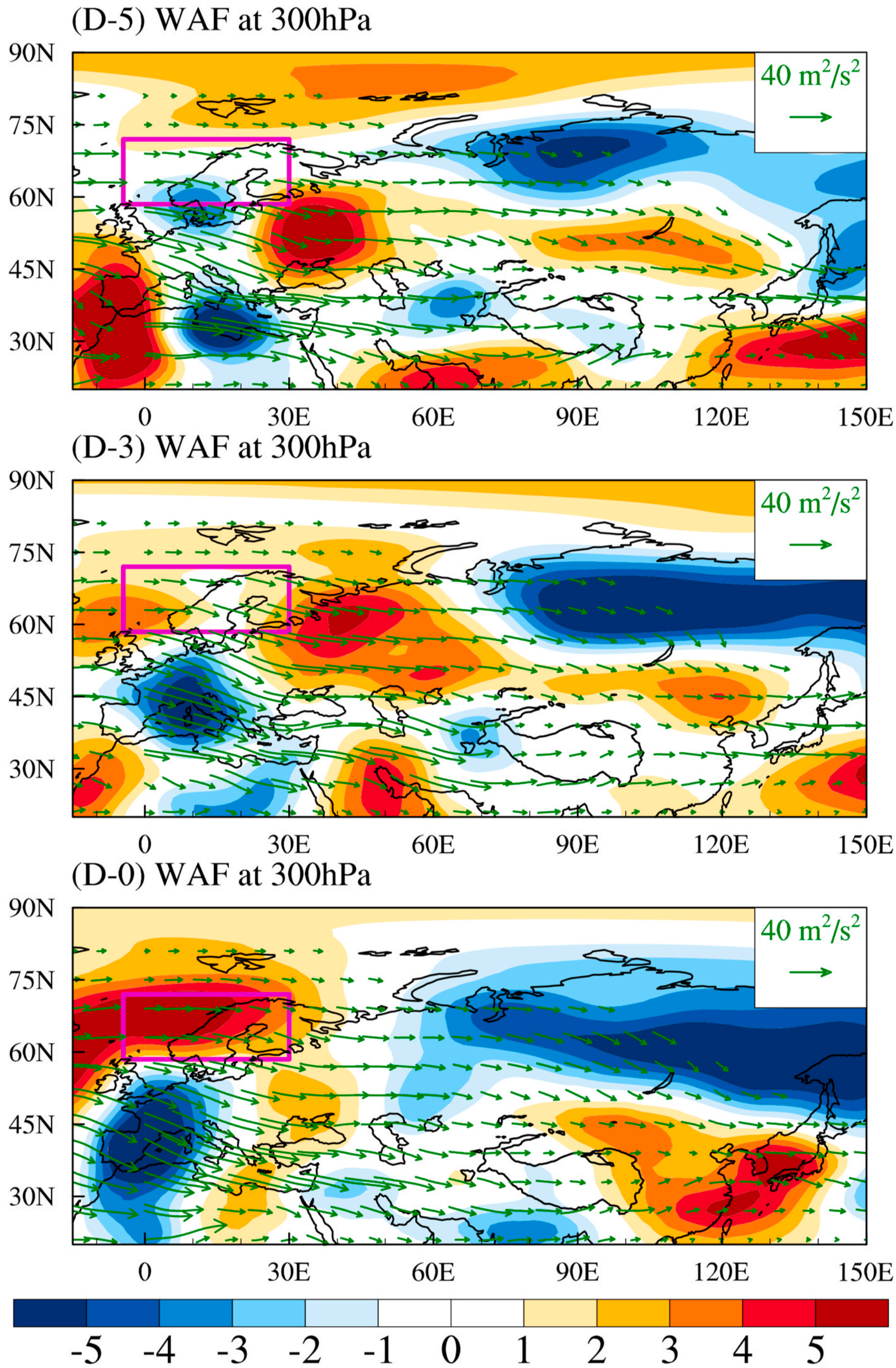

Fig. 6. Composite anomalies of the January quasi-geostrophic stream function (shading, 10^6 m^2/s) and wave activity flux (WAF; vector, m^2/s^2) at 300 hPa before and during the occurrence of EH cases. The pink boxes indicate the eastern North Atlantic and Northern Europe (ENE; 58.5 °N to 72 °N, 4.5 °W to 30 °E). (For interpretation of the references to colour in this figure legend, the reader is referred to the Web version of this article.)

state.

3. Results

3.1. Characteristics of PM_{10} concentration and related atmospheric circulation patterns

The mean and standard deviation of PM_{10} concentrations in South Korea were approximately 56.9 and 22.5 μg/m^3 in January, respectively (Fig. 1). The PM_{10} concentration range during this period was approximately 18.8–206.8 μg/m^3. In particular, the mean and standard deviation of PM_{10} concentrations were high in Seoul and Gyeonggi-do, the metropolitan areas of Korea. Over the past 19 years, the median daily PM_{10} concentration in January was approximately 52.0 μg/m^3, and the 95th percentile value was approximately 100.9 μg/m^3. Based on this information, we divided the daily PM_{10} concentrations into three classes: low (L; < 50 μg/m^3), high (H; 50–100 μg/m^3), and extremely high (EH; ≥100 μg/m^3) (Fig. 1c). The number of H (EH) cases was 287 (30) over the past 19 years, corresponding to 48.7% (5%) of the total number of days (Fig. 1c).

To understand the atmospheric circulation patterns according to the classified PM_{10} concentrations, we investigated the composite patterns

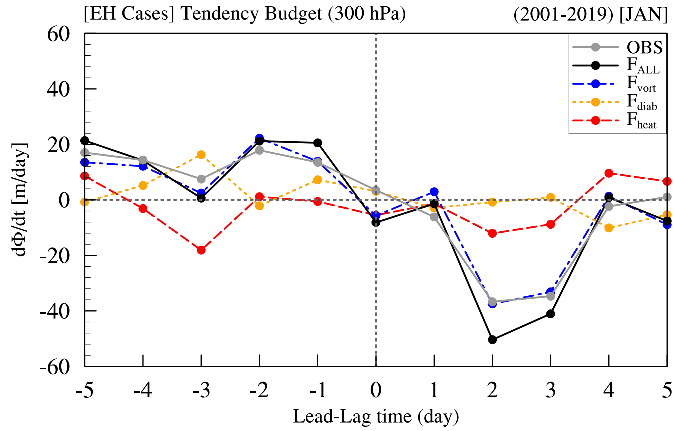

Fig. 7. Time series of geopotential height tendency in the eastern North Atlantic and Northern Europe (ENE; 58.5 °N to 72 °N, 4.5 °W to 30 °E) at 300 hPa. The gray line indicates the tendency obtained from reanalysis data. The black, red, orange, and blue lines indicate the quasi-geostrophic geopotential tendencies induced by the total forcing, temperature advection, diabatic heating, and vorticity forcing, respectively. (For interpretation of the references to colour in this figure legend, the reader is referred to the Web version of this article.)

of each case (Fig. 2). The climatological mean distribution of SLP in January showed that the Siberian high pressure and Aleutian low pressure systems dominated in East Asia, and the Icelandic low pressure and Azores high pressure were predominant in the North Atlantic (Fig. 2a). The SLP variability was high in the North Atlantic Ocean, Kara-Barents seas, and the Ural Mountains, which suggests that these regions may be important for modulating weather patterns in East Asia. The climatological mean distribution of GPH at 300 hPa shows troughs located in Eastern Europe and East Asia (Fig. 2b). During the L cases, the Siberian high pressure and Aleutian low pressure were strengthened in the lower-level atmosphere, and the upper-level trough at 300 hPa also intensified (Fig. 2c). This is similar to the pattern of cold waves over the Korean Peninsula in winter, which is consistent with previous studies (Takaya and Nakamura, 2005; Overland et al., 2015; Heo et al., 2018; Sung and Kim, 2020; Overland et al., 2021). This indicates that strong dispersion due to intensified northerly winds can lower PM_{10} concentrations. In contrast to the cold wave pattern shown in Fig. 2c, H cases are correlated with a weakening of both the Siberian high pressure and Aleutian low pressure at the lower-level, and with an anticyclonic anomaly in the upper-level of the Korean Peninsula (Fig. 2d). In this pattern, the PM_{10} concentration increases as a result of relatively weakened northerly winds and stagnant high pressure in the upper-level atmosphere, as observed in previous studies (Lee et al., 2011; Lee et al., 2018; Kim et al., 2019; Jung et al., 2019).

The circulation patterns during EH cases were noticeably different to that during L and H cases. First, the magnitude of the pressure anomaly was approximately three times larger than that of the L and H cases. Second, the spatial distribution of the anomalies differed, especially in the North Atlantic and Arctic Oceans, with higher GPH anomalies. This suggests that L and H cases in Korea are dominantly affected by the EAWM scale of circulation, whereas EH cases are dominantly influenced by the Eurasian Continental (EC) scale of circulation. Anticyclonic anomalies (anomalous high pressure) cause the atmosphere to stagnate, resulting in increased pollutant concentrations. The PBLH was much shallower during the EH cases than during the L and H cases (Fig. s1), indicating that local meteorological conditions also provide unfavorable conditions for vertical dispersion. Anticyclonic anomalies are dynamically associated with the descending motion that lowers the PBLH (Zhong et al., 2019). Thus, Fig. 2e is consistent with Fig. s1d. This anticyclonic anomaly and the PBLH anomaly are consistent with the temperature inversion (Fig. s2).

As the atmospheric circulation patterns influencing EH cases have not been thoroughly investigated despite their significant impact on society, we focused on EH cases by analyzing the development of EC-scale circulation patterns, particularly in the Atlantic Ocean and Eurasia. Fig. 3 shows the PM_{10} concentration time series five days before and after the occurrence of EH cases. Herein, we defined the first day of 20 EH PM_{10} cases ($\geq$100 μg/m^3) as the start day (lead-lag = 0). The minimum observed PM_{10} concentration during this time series was approximately 44.7 μg/m^3, which was recorded four days before the extreme event. This value then rapidly increased to approximately 117.4 μg/m^3 (2.6 times) over the next four days, which suggests that PM_{10} concentrations in Korea can rapidly increase within just a few days.

As previously discussed, EH cases are associated with EC-scale atmospheric circulation patterns, and PM_{10} concentrations in EH cases can rapidly increase within four days. Therefore, to investigate the development of an EC-scale atmospheric circulation pattern that favors for the occurrence of EH cases, we analyzed the composite anomaly from five days before the start day to the day of occurrence (hereafter, −5 days; Fig. 4). Interestingly, on −5 days, EH cases showed a pressure pattern associated with a cold wave as well as the associated anomalous low surface temperature and northerly winds on the Korean Peninsula. As the EH start day approached, the Siberian high pressure and Aleutian low pressure gradually weakened in the lower-level atmosphere. On the EH start day, the anticyclonic anomaly from the northern part of China moved southward to the Korean Peninsula in the upper-level atmosphere. Anticyclonic anomalies cause the atmosphere to stagnate, resulting in increased pollutant concentrations. Therefore, it is important to understand the mechanisms that induce stagnant anticyclones during EH cases. In addition, the surface temperature was generally warmer, and the anomalous southerly wind was dominant. Furthermore, anticyclonic anomalies emerged in the upper- and lower-level atmosphere in the Norwegian Sea and the Scandinavian Peninsula from three to four days before and substantially grows at the occurrence of EH cases, which had a barotropic structure. This anticyclonic anomaly was the most noticeable difference in the atmospheric circulation

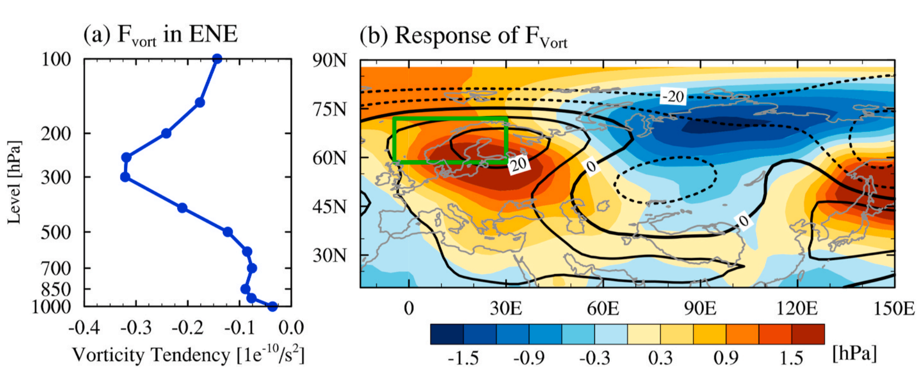

Fig. 8. (a) Vertical distribution of the prescribed vorticity tendency forcing used in the LBM experiment, and (b) model response of sea level pressure (SLP; shading; units: hPa) and geopotential height at 300 hPa (GPH; contour interval of 10 m; units: m; dashed contours are negative). The green box indicates the vorticity tendency forcing region in the eastern North Atlantic and Northern Europe (ENE; 58.5 °N to 72 °N, 4.5 °W to 30 °E). (For interpretation of the references to colour in this figure legend, the reader is referred to the Web version of this article.)

patterns between the H and EH cases. In this study, the region in which the anticyclonic anomaly noticeably appears was defined as the eastern North Atlantic and Northern Europe anticyclonic anomaly region (ENE; 58.5 °N to 72 °N, 4.5 °W to 30 °E).

3.2. Temporal development of North Atlantic forcing

To confirm the development of GPH and TMP in the ENE, we displayed the vertical composite anomaly patterns according to the occurrence days of the EH case (Fig. 5). Notably, four days before the occurrence of EH cases, the anticyclonic anomaly intensified in the upper- and lower-level atmosphere in the ENE, and a strong positive anomaly appeared in the upper-level atmosphere (300 hPa). Moreover, the GPH anomaly in the ENE decayed rapidly one day after the EH start day, which is consistent with the rapid decrease in PM_{10} concentrations, as shown in Fig. 3.

We investigated the propagation path of the Rossby wave in the upper-troposphere (300 hPa) during EH cases using a WAF analysis (Fig. 6). The results showed a weak divergence of WAF from the ENE five days before the EH cases. However, WAF diverged into two branches three days before the EH cases, one from the ENE region to Europe and the other to East Asia along the Siberia. Particularly, the second branch reaches the Korean Peninsula. The rapid growth of the anticyclonic anomalies over the ENE likely plays as a source of the Rossby wave that induces the anomalous atmospheric circulation patterns favorable for the EH cases in the Korean Peninsula.

An anticyclonic anomaly in the ENE, which develops strongly in barotropic structures in the upper- and lower-level atmosphere, was associated with the occurrence of EH cases in Korea. Therefore, we confirmed the QG tendency budget for the presence of remote forcing, which affected the strongly developed anticyclonic anomaly in the ENE (Fig. 7). The solution of the QG tendency budget represents the sum of the three forcings (e.g., vorticity advection, temperature advection, and diabatic heating), and the solution is similar to the QG tendency budget calculated using the reanalyzed data. In the upper-level atmosphere of the ENE, the QG tendency showed positive anomalies before the start day of EH cases, but the QG tendency rapidly decreased from the start day of EH cases. In particular, among the three forcings, the QG tendency due to vorticity advection was the most similar to the QG tendency of all forcings, and the QG tendencies due to diabatic heating and temperature advection were found to cancel each other out. Over the ENE, the GPH anomaly developed four days before the EH case (hereafter, −4 days), and the maximum value appeared on days 0 and + 1 (Fig. 5). According to the QG tendency budget analysis, the tendency term was positive from −4 to −1 days (0 days for reanalysis data) and gradually decreased from −1 days. While the tendency term maintained a positive value, the GPH anomaly accumulated, which increased the positive GPH anomaly. Therefore, Fig. 7 is generally consistent with Fig. 5. The growth of the forcing that triggered the stationary Rossby wave in the ENE also coincided with the growth of the anticyclonic anomaly over the Korean Peninsula, leading to a maximum at 0 days. These results indicate that the anticyclonic anomaly strongly developed in the upper-level atmosphere of the ENE is dominantly influenced by vorticity advection forcing.

3.3. Linear baroclinic modeling experiment

We conducted an LBM experiment to confirm whether the anticyclonic anomaly developed over the ENE induces the EC-scale atmospheric circulation pattern related to EH cases in Korea (Fig. 8). In this experiment, we prescribed the mean tendency of vorticity advection on −4 to −1 days to reproduce the averaged response of the atmospheric circulation over Eurasia. The results of the LBM experiment showed a strongly developed anticyclonic anomaly in the upper- and lower-level atmosphere over the ENE, as well as the development of negative and positive anomalies in Siberia and East Asia, respectively (Fig. 8b). In addition, the southeasterly winds dominate in the lower-level troposphere over the Korean Peninsula. This lower-tropospheric circulation pattern provides favorable condition for EH cases by weakening the seasonal northwesterly prevailing during the winter (Lee et al., 2020a). This pattern is consistent with the observed pattern shown in Fig. 2e. This suggests that the negative vorticity advection in the ENE induced the observed EC-scale atmospheric circulation pattern, which is favorable for EH cases on the Korean Peninsula.

Vorticity advection in the ENE may have various causes, such as the North Atlantic Oscillation (NAO) and sea surface temperature variability in the North Atlantic (Hurrell and Deser, 2010; Comas-Bru and McDermott, 2014). In particular, NAO is a dominant mode of climate variability in Europe and North America. Therefore, we investigated the potential links between EH cases and the NAO (Fig. s3) and found that the circulation anomalies for the negative and positive NAO phases were not consistent with those of the EH cases. Interestingly, the circulation anomaly of the neutral NAO phase was similar to that of the EH cases (Fig. s3b), indicating that the teleconnection via ENE forcing is effective when the NAO is neutral.

4. Conclusion

In this study, we classified the daily PM_{10} concentrations into three classes using the median and 95th percentile values: L cases (<50 μg/m^3), H cases (50–100 μg/m^3), and EH cases (≥100 μg/m^3). Our results clearly showed that a strengthening (weakening) EAWM on the Asian monsoon scale influenced the PM_{10} concentrations during L (H) cases. Interestingly, EH cases showed strong anomaly patterns on EC-scale atmospheric circulation, which was distinct from that of the L and H cases.

The ENE was the key region affecting the occurrence of EH cases, which corresponds to the North Atlantic Ocean, including the Norwegian Sea and the Scandinavian Peninsula. The rapid growth of the barotropic warming anomaly over the ENE weakens the trough in the upper troposphere over the Korean Peninsula through stationary Rossby waves in the upper-level atmosphere; this induces a shallower PBLH and weakens the wind speed. As a result, the PM_{10} concentration during EH cases sharply increased by ~2.6 times from 44.7 μg/m^3 to 117.4 μg/m^3 in just four days. Our findings highlight the importance of understanding the teleconnection between ENE forcing and EC-scale atmospheric conditions for predicting the occurrence of EH cases in Korea and reducing the human health risks of atmospheric pollution.

Author statement

Jeong-Hun Kim: Conceptualization, Formal Analysis, Investigation, Methodology, Visualization, Writing—Original Draft. Seong-Joong Kim: Conceptualization, Investigation, Methodology, Writing—Review & Editing. Daeok Yun: Investigation, Methodology, Writing—Review & Editing. Maeng-Ki Kim: Conceptualization, Investigation, Methodology, Writing—Review & Editing. Joo-Hong Kim: Methodology, Writing—Review & Editing. Joowan Kim: Methodology, Writing—Review & Editing. El Noh: Methodology, Writing—Review & Editing.

Declaration of competing interest

The authors declare that they have no known competing financial interests or personal relationships that could have appeared to influence the work reported in this paper.

Acknowledgments

This work was supported by the Korea Polar Research Institute (KOPRI) project entitled "Earth System Model-based Korea Polar Prediction System (KPOPS-Earth) Development and Its Application to the High-impact Weather Events originated from the Changing Arctic Ocean and Sea Ice” (PE21010) and the Korea Meteorological Administration Research and Development Program under Grant KMI(KMI2020-01414).

Appendix A. Supplementary data

Supplementary data to this article can be found online at https://doi.org/10.1016/j.envpol.2021.118051.

References

Bae, M., Kim, B.U., Kim, H.C., Kim, J., Kim, S., 2021. Role of emissions and meteorology in the recent PM2.5 changes in China and South Korea from 2015 to 2018. Environ. Pollut. 270, 116233. https://doi.org/10.1016/j.envpol.2020.116233.

Brunekreef, B., Holgate, S.T., 2002. Air pollution and health. Lancet 360, 1233–1242. https://doi.org/10.1016/S0140-6736(02)11274-8.

Cai, W., Li, K., Liao, H., Wang, H., Wu, L., 2017. Weather conditions conducive to Beijing severe haze more frequent under climate change. Nat. Clim. Change 7, 257–262. https://doi.org/10.1038/nclimate3249.

Chen, C., Su, M., Liu, G., Yang, Z., 2013. Evaluation of economic loss from energy-related environmental pollution: a case study of Beijing. Front. Earth Sci. 7, 320–330. https://doi.org/10.1007/s11707-013-0360-4.

Comas-Bru, L., McDermott, F., 2014. Impacts of the EA and SCA patterns on the European twentieth century NAO-winter climate relationship. Q. J. R. Meteorol. Soc. 140, 354–363. https://doi.org/10.1002/qj.2158.

Dotse, S.Q., Dagar, L., Petra, M.I., De Silva, L.C., 2016. Influence of southeast asian haze episodes on high PM10 concentrations across Brunei Darussalam. Environ. Pollut. 219, 337–352. https://doi.org/10.1016/j.envpol.2016.10.059.

Du, Y., Li, T., 2016. Assessment of health-based economic costs linked to fine particulate (PM2.5) pollution: a case study of haze during January 2013 in Beijing, China. Air Qual. Atmos. Heal. 9, 439–445. https://doi.org/10.1007/s11869-015-0387-7.

Guan, Q., Cai, A., Wang, F., Yang, L., Xu, C., Liu, Z., 2017. Spatio-temporal variability of particulate matter in the key part of Gansu Province, Western China. Environ. Pollut. 230, 189–198. https://doi.org/10.1016/j.envpol.2017.06.045.

He, C., Liu, R., Wang, X., Liu, S.C., Zhou, T., Liao, W., 2019. How does El Niño-Southern Oscillation modulate the interannual variability of winter haze days over eastern China? Sci. Total Environ. 651, 1892–1902. https://doi.org/10.1016/j.scitotenv.2018.10.100.

Heo, J.W., Ho, C.H., Park, T.W., Choi, W., Jeong, J.H., Kim, J., 2018. Changes in cold surge occurrence over East Asia in the future: role of thermal structure. Atmosphere 9, 1–16. https://doi.org/10.3390/atmos9060222.

Holton, J.R., 2004. An Introduction to Dynamic Meteorology, fourth ed. Academic Press, p. 535.

Hur, S.K., Ho, C.H., Kim, J., Oh, H.R., Koo, Y.S., 2021. Systematic bias of WRF-CMAQ PM10 simulations for Seoul, Korea. Atmos. Environ. 244, 117904. https://doi.org/10.1016/j.atmosenv.2020.117904.

Hurrell, J.W., Deser, C., 2010. North Atlantic climate variability: the role of the north atlantic oscillation. J. Mar. Syst. 79, 231–244. https://doi.org/10.1016/j.jmarsys.2009.11.002.

Hwang, J., Martineau, P., Son, S.W., Miyasaka, T., Nakamura, H., 2020. The role of transient eddies in north pacific blocking formation and its seasonality. J. Atmos. Sci. 77, 2453–2470. https://doi.org/10.1175/JAS-D-20-0011.1.

Jeong, J.I., Park, R.J., 2017. Winter monsoon variability and its impact on aerosol concentrations in East Asia. Environ. Pollut. 221, 285–292. https://doi.org/10.1016/j.envpol.2016.11.075.

Jung, M.I., Son, S.W., Kim, H.C., Kim, S.W., Park, R.J., Chen, D., 2019. Contrasting synoptic weather patterns between non-dust high particulate matter events and Asian dust events in Seoul, South Korea. Atmos. Environ. 214, 116864. https://doi.org/10.1016/j.atmosenv.2019.116864.

Kim, H.C., Kim, S., Son, S.W., Lee, P., Jin, C.S., Kim, E., Kim, B.U., Ngan, F., Bae, C., Stein, A., 2016. Synoptic perspectives on pollutant transport patterns observed by satellites over East Asia: case studies with a conceptual model. Atmos. Chem. Phys. Discuss. 1–30. https://doi.org/10.5194/acp-2016-673.

Kim, H.C., Kim, S., Kim, B.U., Jin, C.S., Hong, S., Park, R., Son, S.W., Bae, C., Bae, M., Song, C.K., Stein, A., 2017a. Recent increase of surface particulate matter concentrations in the Seoul Metropolitan Area, Korea. Sci. Rep. 7, 1–7. https://doi.org/10.1038/s41598-017-05092-8.

Kim, H.C., Kim, E., Bae, C., Cho, J.H., Kim, B.U., Kim, S., 2017b. Regional contributions to particulate matter concentration in the Seoul metropolitan area, South Korea: seasonal variation and sensitivity to meteorology and emissions inventory. Atmos. Chem. Phys. 17, 10315–10332. https://doi.org/10.5194/acp-17-10315-2017.

Kim, J.H., Kim, M.K., Ho, C.H., Park, R.J., Kim, M.J., Lim, J., Kim, S.J., Song, C.K., 2019. Possible link between Arctic sea ice and January PM10 concentrations in South Korea. Atmosphere 10, 1–15. https://doi.org/10.3390/atmos10100619.

Koo, Y.S., Yun, H.Y., Choi, D.R., Han, J.S., Lee, J.B., Lim, Y.J., 2018. An analysis of chemical and meteorological characteristics of haze events in the Seoul metropolitan area during January 12–18, 2013. Atmos. Environ. 178, 87–100. https://doi.org/10.1016/j.atmosenv.2018.01.037.

Korea Ministry of Environment, 2015. The 4th National Environmental Comprehensive Plan for 2016–2035. Korea Ministry of Environment. http://eng.me.go.kr/eng/file/readDownloadFile.do?fileId=115224&fileSeq=1&openYn=Y. (Accessed 28 April 2021).

Ku, H., Noh, N., Jeong, J., Koo, J., Choi, W., Kim, B., Lee, D., Ban, S., 2021. Classification of large-scale circulation patterns and their spatio-temporal variability during High-PM 10 events over the Korean Peninsula. Atmos. Environ. 262 (July), 118632. https://doi.org/10.1016/j.atmosenv.2021.118632.

Kwon, S.H., Kim, J., Shim, S., Seo, J., Byun, Y.H., 2020. Analysis of weather patterns related to wintertime particulate matter concentration in seoul and a cmip6-based air quality projection. Atmosphere 11. https://doi.org/10.3390/atmos11111161.

Lee, S., Ho, C.H., Choi, Y.S., 2011. High-PM10 concentration episodes in Seoul, Korea: background sources and related meteorological conditions. Atmos. Environ. 45, 7240–7247. https://doi.org/10.1016/j.atmosenv.2011.08.071.

Lee, S., Ho, C.H., Lee, Y.G., Choi, H.J., Song, C.K., 2013. Influence of transboundary air pollutants from China on the high-PM10 episode in Seoul, Korea for the period October 16-20, 2008. Atmos. Environ. 77, 430–439. https://doi.org/10.1016/j.atmosenv.2013.05.006.

Lee, H.J., Jeong, Y.M., Kim, S.T., Lee, W.S., 2018. Atmospheric circulation patterns associated with particulate matter over South Korea and their future projection. J. Clim. Chang. Res. 9, 423–433. https://doi.org/10.15531/ksccr.2018.9.4.423.

Lee, J., Kim, K.Y., 2018. Analysis of source regions and meteorological factors for the variability of spring PM10 concentrations in Seoul, Korea. Atmos. Environ. 175, 199–209. https://doi.org/10.1016/j.atmosenv.2017.12.013.

Lee, D., Wang, S.Y., Simon, Zhao, L., Kim, H.C., Kim, K., Yoon, J.H., 2020a. Long-term increase in atmospheric stagnant conditions over northeast Asia and the role of greenhouse gases-driven warming. Atmos. Environ. 241, 117772. https://doi.org/10.1016/j.atmosenv.2020.117772.

Lee, G., Ho, C.H., Chang, L.S., Kim, J., Kim, M.K., Kim, S.J., 2020b. Dominance of large-scale atmospheric circulations in long-term variations of winter PM10 concentrations over East Asia. Atmos. Res. 238, 104871. https://doi.org/10.1016/j.atmosres.2020.104871.

Nel, A., 2005. Air pollution – related illness: effects of particles. Science 308 (5723), 804–806. https://doi.org/10.1126/science.309.5739.1326a.

Niu, F., Li, Z., Li, C., Lee, K.H., Wang, M., 2010. Increase of wintertime fog in China: potential impacts of weakening of the Eastern Asian monsoon circulation and increasing aerosol loading. J. Geophys. Res. Atmos. 115, 1–12. https://doi.org/10.1029/2009JD013484.

Oh, H.R., Ho, C.H., Kim, J., Chen, D., Lee, S., Choi, Y.S., Chang, L.S., Song, C.K., 2015. Long-range transport of air pollutants originating in China: a possible major cause of multi-day high-PM10 episodes during cold season in Seoul, Korea. Atmos. Environ. 109, 23–30. https://doi.org/10.1016/j.atmosenv.2015.03.005.

Oh, H.R., Ho, C.H., Park, D.S.R., Kim, J., Song, C.K., Hur, S.K., 2018. Possible relationship of weakened Aleutian low with air quality improvement in Seoul, South Korea. J. Appl. Meteorol. Climatol. 57, 2363–2373. https://doi.org/10.1175/JAMC-D-17-0308.1.

Oh, H.R., Ho, C.H., Koo, Y.S., Baek, K.G., Yun, H.Y., Hur, S.K., Choi, D.R., Jhun, J.G., Shim, J.S., 2020. Impact of Chinese air pollutants on a record-breaking PMs episode in the Republic of Korea for 11–15 January 2019. Atmos. Environ. 223, 117262. https://doi.org/10.1016/j.atmosenv.2020.117262.

Overland, J., Francis, J.A., Hall, R., Hanna, E., Kim, S.J., Vihma, T., 2015. The melting arctic and midlatitude weather patterns: are they connected? J. Clim. 28, 7917–7932. https://doi.org/10.1175/JCLI-D-14-00822.1.

Overland, J.E., Ballinger, T.J., Cohen, J., Francis, J.A., Hanna, E., Jaiser, R., Kim, B.M., Kim, S.J., Ukita, J., Vihma, T., Wang, M., Zhang, X., 2021. How do intermittency and simultaneous processes obfuscate the Arctic influence on midlatitude winter extreme weather events? Environ. Res. Lett. 16 https://doi.org/10.1088/1748-9326/abdb5d.

Park, S.U., Cho, J.H., Park, M.S., 2013. Analyses of high aerosol concentration events (dense haze/mist) occurred in East Asia during 10-16 January 2013 using the data simulated by the Aerosol Modeling System. Int. J. Chem. 10–26, 03. https://citeseerx.ist.psu.edu/viewdoc/download?doi=10.1.1.399.7297&rep=rep1&type=pdf. (Accessed 21 June 2021).

Rai, P., Furger, M., Slowik, J.G., Zhong, H., Tong, Y., Wang, L., Duan, J., Gu, Y., Qi, L., Huang, R.J., Cao, J., Baltensperger, U., Prévôt, A.S.H., 2021. Characteristics and sources of hourly elements in PM10 and PM2.5 during wintertime in Beijing. Environ. Pollut. 278 https://doi.org/10.1016/j.envpol.2021.116865.

Ryou, H., Heo, J., Kim, S.Y., 2018. Source apportionment of PM10 and PM2.5 air pollution, and possible impacts of study characteristics in South Korea. Environ. Pollut. 240, 963–972. https://doi.org/10.1016/j.envpol.2018.03.066.

Seo, J., Kim, J.Y., Youn, D., Lee, J.Y., Kim, H., Lim, Y. Bin, Kim, Y., Cher Jin, H., 2017. On the multiday haze in the Asian continental outflow: the important role of synoptic conditions combined with regional and local sources. Atmos. Chem. Phys. 17, 9311–9332. https://doi.org/10.5194/acp-17-9311-2017.

Seo, J., Park, D.S.R., Kim, J.Y., Youn, D., Lim, Y. Bin, Kim, Y., 2018. Effects of meteorology and emissions on urban air quality: a quantitative statistical approach to long-term records (1999-2016) in Seoul, South Korea. Atmos. Chem. Phys. 18, 16121–16137. https://doi.org/10.5194/acp-18-16121-2018.

Shi, P., Zhang, G., Kong, F., Chen, D., Azorin-Molina, C., Guijarro, J.A., 2019. Variability of winter haze over the Beijing-Tianjin-Hebei region tied to wind speed in the lower troposphere and particulate sources. Atmos. Res. 215, 1–11. https://doi.org/10.1016/j.atmosres.2018.08.013.

Sung, H.J., Kim, B.M., 2020. Regional characteristics of cold surges over the South Korea. Atmosphere 30 (3), 249–256. https://doi:10.14191/ATMOS.2020.30.3.249.

Takaya, K., Nakamura, H., 2001. A formulation of a phase-independent wave-activity flux for stationary and migratory quasigeostrophic eddies on a zonally varying basic flow. J. Atmos. Sci. 58, 608–627. https://doi.org/10.1175/1520-0469(2001)058<0608:AFOAPI>2.0.CO;2.

Takaya, K., Nakamura, H., 2005. Mechanisms of intraseasonal amplification of the cold Siberian high. J. Atmos. Sci. 62, 4423–4440. https://doi.org/10.1175/JAS3629.1.

Wang, H., Xu, J., Zhang, M., Yang, Y., Shen, X., Wang, Y., Chen, D., Guo, J., 2014. A study of the meteorological causes of a prolonged and severe haze episode in January 2013 over central-eastern China. Atmos. Environ. 98, 146–157. https://doi.org/10.1016/j.atmosenv.2014.08.053.

Wang, H.J., Chen, H.P., 2016. Understanding the recent trend of haze pollution in eastern China: roles of climate change. Atmos. Chem. Phys. 16 (6), 4205–4211. https://doi.org/10.5194/acp-16-4205-2016.

Wang, H.J., Chen, H.P., Liu, J., 2015. Arctic sea ice decline intensified haze pollution in eastern China. Atmos. Oceanogr. Sci. Libr. 8, 1–9. https://doi.org/10.3878/AOSL20140081.

Watanabe, M., Kimoto, M., 2000. Atmosphere-ocean thermal coupling in the North Atlantic: a positive feedback. Q. J. R. Meteorol. Soc. 126, 3343–3369. https://doi.org/10.1256/smsqj.57016.

Wie, J., Moon, B.K., 2017. ENSO-related PM10 variability on the Korean Peninsula. Atmos. Environ. 167, 426–433. https://doi.org/10.1016/j.atmosenv.2017.08.052.

Zhao, S., Feng, T., Tie, X., Long, X., Li, G., Cao, J., Zhou, W., An, Z., 2018. Impact of climate change on siberian high and wintertime air pollution in China in past two decades. Earth's Futur 6, 118–133. https://doi.org/10.1002/2017EF000682.

Zhong, W., Yin, Z., Wang, H., 2019. The relationship between anticyclonic anomalies in northeastern Asia and severe haze in the Beijing-Tianjin-Hebei region. Atmos. Chem. Phys. 19, 5941–5957. https://doi.org/10.5194/acp-19-5941-2019.

Zou, Y., Wang, Y., Zhang, Y., Koo, J.H., 2017. Arctic sea ice, Eurasia snow, and extreme winter haze in China. Sci. Adv. 3 https://doi.org/10.1126/sciadv.1602751.